Simultaneous ODF Estimation and Tractography in HARDI*

H. Ertan Çetingül[1], Mariappan Nadar[1], Paul Thompson[2], Guillermo Sapiro[3], and Christophe Lenglet[3]

***Abstract*— We consider the problem of tracking white matter fibers in high angular resolution diffusion imaging (HARDI) data while simultaneously estimating the local fiber orientation profile. Prior work showed that an unscented Kalman filter (UKF) can be used for this problem, yet existing algorithms employ parametric mixture models to represent water diffusion and to define the state space. To address this restrictive model dependency, we propose to extend the UKF to HARDI data modeled by orientation distribution functions (ODFs), a more generic diffusion model. We consider the spherical harmonic representation of the HARDI signal as the state, enforce nonnegativity of the ODFs, and perform tractography using the directions at which the ODFs attain their peaks. In simulations, our method outperforms filtered two-tensor tractography at different levels of noise by achieving a reduction in mean Chamfer error of 0.05 to 0.27 voxels; it also produced in vivo fiber tracking that is consistent with the neuroanatomy.**

I. Introduction

Quantitative characterization of the brain circuitry is an important problem in neuroradiology as damage to this circuitry may indicate neurological disease. Diffusion magnetic resonance imaging (DMRI) is presently the only available noninvasive technique to investigate white matter (WM) architecture in vivo. DMRI produces images of biological tissues by measuring the anisotropic diffusion of water molecules and the WM fiber orientations can be inferred from the directions of maximum diffusion. State-of-the-art DMRI techniques such as high angular resolution diffusion imaging (HARDI) enables the reconstruction of the orientation distribution function (ODF) [1], [2], which offers improved accuracy in resolving intra-voxel complexities over the diffusion tensor (DT) model [3], currently the de facto standard for clinical applications.

Prior work on tractography often estimates a diffusion model at each spatial location and then delineates the tracts via deterministic or probabilistic methods (see [4]–[8] and references therein). Yet, if tracking is considered as a causal process (e.g., in common deterministic approaches), model estimation and tractography can be unified in a process recast within a causal filter, as demonstrated in [9]. More specifically, [9] proposes to use an unscented Kalman filter (UKF) for which the parameters of a multi-tensor model, i.e., mixtures of diffusion tensors, form the state space. By examining the measured signal at a location, the filter recursively updates the parameters of the local model, provides the covariance of that estimate, and indicates the most consistent direction for tracking. In theory, this strategy, known as "filtered multi-tensor tractography," is fast (since it avoids estimation at every voxel) and robust to noise (due to the nature of filtering).

Filtered multi-tensor tractography [9] assumes an underlying diffusion model (i.e., a rank-2 tensor) with fixed number of mixtures. This results in a state space representation where the state vector is the fusion of several elements (e.g., principal eigenvectors-eigenvalues and mixture weights) with different statistical properties. Thus, parameter tuning and preservation of physically meaningful states during the evolution are vital for robustness, as discussed in [10]. In this work, we propose to extend the UKF framework to HARDI data modeled by ODFs, a more generic and versatile representation of diffusion. We consider the spherical harmonic representation of ODFs as the state and enforce nonnegativity of the ODFs during the evolution. We use mean shift clustering [11] on the 2-sphere $\mathbb{S}^2$ to identify the directions at which the ODFs attain their peaks and perform deterministic tractography. We evaluate the performance of our method on synthetic and real data.

II. Filtered ODF Tractography

A. Diffusion Representation with Spherical Harmonics

DMRI quantifies the anisotropy of water diffusion by measuring the HARDI signal attenuation S along N different gradient directions $\{(\theta_n, \phi_n)\}_{n=1}^{N} \subset \mathbb{S}^2$. The signal is mostly attenuated in regions where WM tracts are oriented along a given direction. Let S_0 denote the baseline signal with no diffusion sensitization, and let S_n be the HARDI signal in the gradient direction (θ_n, ϕ_n). To represent the local diffusion, we consider the single shell Q-ball imaging formulation in [2], where the ODF in the spatial direction (ϑ, φ) is given by

$$p(\vartheta, \varphi) = \frac{1}{4\pi} + \frac{1}{16\pi^2} \mathsf{FRT}\Big\{ \nabla_b^2 \ln\Big(-\ln\Big(\frac{S_n}{S_0}\Big)\Big)\Big\}. \quad (1)$$

Here, FRT is the Funk-Radon transform and ∇_b^2 is the Laplace-Beltrami operator on $\mathbb{S}^2$, which is independent of the radial component. Since spherical harmonics (SHs) are eigenfunctions of the Laplace-Beltrami operator and the Funk-Radon transform, and S is assumed real and antipodally symmetric, one can use the approximation

$$\ln\Big(-\ln\Big(\frac{S_n}{S_0}\Big)\Big) \approx \sum_{t=1}^{T} c_t Y_t(\theta_n, \phi_n), \quad (2)$$

*Work supported in part by NIH grants R01 EB008432, P41 RR008079 (NCRR), P41 EB015894 (NIBIB), P30 NS057091, P30 NS5076408 and the Human Connectome Project (U54 MH091657) from the 16 NIH Institutes and Centers that support the NIH Blueprint for Neuroscience Research.

[1]H.E. Çetingül (corresponding author) and M. Nadar are with Siemens Corporation, Corporate Research and Technology, Princeton, NJ 08540, USA (e-mail: {hasan.cetingul, mariappan.nadar} at siemens.com).

[2]P. Thompson is with the Laboratory of Neuro Imaging, University of California at Los Angeles (UCLA), Los Angeles, CA 90095, USA (e-mail: thompson at loni.ucla.edu).

[3]G. Sapiro and C. Lenglet are respectively with the Department of Electrical & Computer Engineering and the Center for Magnetic Resonance Research, University of Minnesota, MN 55455, USA (e-mail: {guille, clenglet} at umn.edu).

where $c_t \in \mathbb{R}$ is the SH coefficient associated with the modified SH function

$$Y_t = \begin{cases} \sqrt{2}\text{Re}\{Y_l^{|m|}\} & \text{if } -l \le m < 0, \\ Y_l^m & \text{if } m = 0, \\ \sqrt{2}(-1)^{m+1}\text{Im}\{Y_l^m\} & \text{if } 0 < m \le l. \end{cases} \quad (3)$$

There are $T=(L+1)(L+2)/2$ such functions for the SH basis of degree L with indices $t(l,m)=(l^2+l+2)/2+m$, where $l=0,2,\ldots,L$, $|m|\le l$, and $\text{Re}\{Y_l^m\}$ and $\text{Im}\{Y_l^m\}$ are respectively the real and imaginary parts of the standard SH basis function $Y_l^m : \mathbb{S}^2 \to \mathbb{C}$ of degree l and order m [12]. In this work, we consider the SH basis of degree $L=4$ (i.e., with $T=15$), and write (2) in vector form as

$$s_n \doteq \ln\Big(-\ln\Big(\frac{S_n}{S_0}\Big)\Big) \approx \big[Y_1(\theta_n,\phi_n),\ldots,Y_{15}(\theta_n,\phi_n)\big]\mathbf{c}. \quad (4)$$

Once the least-squares solution of (4) for the unknown $\mathbf{c} \in \mathbb{R}^T$ is found, a discrete representation of the ODF can be reconstructed as described in [2], [13]. The method in [13] also enforces the estimated ODFs to be nonnegative and it is used, in this work, to initialize the proposed algorithm.

B. WM Tractography using the Unscented Kalman Filter

The main idea in filtered tractography is to estimate and recursively update the diffusion model given the signal at a spatial location and trace the fiber by propagating in the most consistent direction. If one uses a state-space filter, e.g., the Kalman filter, for tractography, the four components of this filter are the *system state* $\mathbf{x}$ (diffusion model), the *state transition function*, f (to predict how the diffusion model changes during fiber tracking), the *observation function*, h (to predict the signal for a particular state), and the *measurement* $\mathbf{y}$ (the acquired HARDI signal). We consider the SH coefficient vector $\mathbf{c}$ as the state, i.e., $\mathbf{x}=\mathbf{c}=\big[c_1,c_2,\ldots,c_T\big]^\top$, and identity dynamics for the state transition f assuming that the diffusion profile does not change drastically in the vicinity of a location of interest (spatial regularity). The measurement $\mathbf{y}$ is the HARDI signal S at that location, and the observation h is the reconstruction of the signal from (4).

Since the signal reconstruction in (2) is nonlinear, the unscented Kalman filter (UKF) is a more appropriate choice for filtered tractography. The UKF uses a deterministic sampling technique known as the *unscented transform* (UT), which calculates the statistics (mean and covariance) of a random variable undergoing a nonlinear transformation. The filter first uses the state transition model to *predict* the next state and observation, and then uses the measurement to *update* the state estimate. One iteration of this recursive algorithm can be outlined as follows. Let $\mathbf{x}_k \in \mathbb{R}^T$ and $P_k \in \mathbb{R}^{T\times T}$ be the estimated mean and covariance matrix of the current state at discrete time k. In the prediction stage, a set $\mathcal{X}_k$ of $2T+1$ *sigma points* $\{\chi_i\} \subset \mathbb{R}^T$ with weights

$$w_0 = \frac{\kappa}{T+\kappa},\ w_i = w_{i+T} = \frac{1}{2(T+\kappa)},$$

are spread around $\mathbf{x}_k$ such that $\chi_0=\mathbf{x}_k$ and

$$\chi_i = \mathbf{x}_k + \Big[\sqrt{(T+\kappa)P_k}\Big]_i,\quad \chi_{i+T} = \mathbf{x}_k - \Big[\sqrt{(T+\kappa)P_k}\Big]_i.$$

Here, $[A]_i$ denotes the i-th column of the matrix A and κ is a scaling parameter set to 0.01. Next, the predicted sample set of states $\mathcal{X}_{k+1|k}$ is obtained by propagating $\mathcal{X}_k$ through the state transition function, i.e., $\mathcal{X}_{k+1|k} = \{f(\chi_i)\} = \{\hat{\chi}_i\}$. The resulting set is used to calculate the predicted system mean state $\hat{\mathbf{x}}_{k+1|k} = \sum_i w_i\hat{\chi}_i$, and covariance $P_{xx} = \sum_i w_i(\hat{\chi}_i - \hat{\mathbf{x}}_{k+1|k})(\hat{\chi}_i - \hat{\mathbf{x}}_{k+1|k})^\top + Q_{\mathbf{c}}$, where $Q_{\mathbf{c}} \in \mathbb{R}^{T\times T}$ is the covariance of the process noise. Then the predicted set of observations is obtained as $\mathcal{Y}_{k+1|k} = \{h(\hat{\chi}_i)\} = \{\gamma_i\}$. These observations are used to calculate the mean $\hat{\mathbf{y}}_{k+1|k} = \sum_i w_i\hat{\gamma}_i$, and covariance $P_{yy} = \sum_i w_i(\hat{\gamma}_i - \hat{\mathbf{y}}_{k+1|k})(\hat{\gamma}_i - \hat{\mathbf{y}}_{k+1|k})^\top + R_{\mathbf{s}}$, where $R_{\mathbf{s}} \in \mathbb{R}^{N\times N}$ is the covariance of the measurement noise. Finally, the Kalman gain $K = P_{xy}P_{yy}^{-1} \in \mathbb{R}^{T\times N}$, with $P_{xy} = \sum_i w_i(\hat{\chi}_i - \hat{\mathbf{x}}_{k+1|k})(\hat{\gamma}_i - \hat{\mathbf{y}}_{k+1|k})^\top$ being the cross correlation between the state and observation, is used to correct our prediction and obtain the updated state mean $\mathbf{x}_{k+1}$ and covariance P_{k+1},

$$\mathbf{x}_{k+1} = \hat{\mathbf{x}}_{k+1|k} + K(\mathbf{y}_t - \hat{\mathbf{y}}_{k+1|k}), \quad (5)$$

$$P_{k+1} = P_{xx} - KP_{yy}K^\top. \quad (6)$$

C. Summary and Implementation Details

1) Outline of the Algorithm: The proposed algorithm is initialized, at user- (or mask image-) specified seed points, by estimating the SH representation of the HARDI signal and reconstructing the ODFs as described in [13] and summarized in §II-A. For each seed point on the fiber to be tracked, the resulting SH coefficient vector $\mathbf{c}$ is taken as the initial state $\mathbf{x}_0$ and the number and locations of the mode(s) of the ODF are identified via weighted spherical mean shift clustering [11]. The resulting modes represent the candidate directions to be followed at the current location. At the k-th iteration, we predict the new state as $\mathbf{x}_{k+1|k} = f(\mathbf{x}_k) = \mathbf{x}_k$, use the observation $h : \mathbb{R}^T \to \mathbb{R}^N$ of the form

$$S_n = S_0 \exp\Big(-\exp\Big(\sum_t c_t Y_t(\theta_n,\phi_n)\Big)\Big), \quad (7)$$

for $n=1,2,\ldots,N$, along with the measured signal interpolated at the current spatial location, and compute the new state $\mathbf{x}_{k+1}$. This estimate is used to reconstruct the ODF whose modes (directions to be followed at $k+1$) are subsequently identified. We use second-order Runge-Kutta path integration strategy to propagate forward in the direction consistent with the previous direction of propagation and repeat this procedure until user-defined termination criteria (e.g., high curvature, maximum length, low generalized fractional anisotropy) are met. To enforce nonnegativity of the estimated ODFs (at the initialization and at the end of each iteration), we employ the constrained optimization strategy proposed in [13].

2) Parameter Selection: The UKF framework requires a few parameters to be tuned, namely the covariance matrices of the process noise and measurement noise, $Q_{\mathbf{c}}$ and $R_{\mathbf{s}}$, respectively. We assume that these matrices are diagonal with entries $q_{\mathbf{c}}=0.01$ and $r_{\mathbf{s}}=0.02$, respectively, but at the same time we observe that the algorithm is robust for different (yet comparable) values of these parameters.

III. Validation and Discussions

A. Experiments on Synthetic Data

Experiments on synthetic data evaluate the sensitivity of our method to noise and compare its performance to that of the filtered two-tensor tractography method with the parameter settings given in [9]. We generate a synthetic dataset comprising diffusion weighted images of 60 fiber configurations. Each configuration has two randomly generated fibers that intersect. The centerline of each fiber is formed by fitting cubic splines through at most three randomly selected points in a 30×30 lattice. As a result, we obtain configurations at different levels of complexity, which include intersecting linear or curved fibers (see Fig. 1(a)). We use the two-tensor model in [12], where the HARDI signals $\{S_n\}_{n=1}^{N}$ at $N = 81$ gradient directions, with $S_0 = 1$ and $b = 2{,}000$ s/mm^2, are simulated to represent an isotropic background and ODFs of 1 or 2 fibers according to the shape of a fiber centerline. Noisy signals are generated by adding Rician (complex Gaussian) noise with zero mean and standard deviation $\sigma = S_0/\zeta$, where ζ is the signal-to-noise ratio (SNR).

Accuracy in tracking is quantified by the spatial tracking error (in voxels) computed as the symmetrized Chamfer distance $\epsilon(\mathfrak{X}^e, \mathfrak{X}^t)$ between the estimated tract $\mathfrak{X}^e = (x_1^e, x_2^e, \dots)$ and the ground truth centerline $\mathfrak{X}^t = (x_1^t, x_2^t, \dots)$, i.e.,

$$\epsilon(\mathfrak{X}^e, \mathfrak{X}^t) = \frac{1}{2}\big(d_{\text{Chamfer}}(\mathfrak{X}^e, \mathfrak{X}^t) + d_{\text{Chamfer}}(\mathfrak{X}^t, \mathfrak{X}^e)\big), \quad (8)$$

$$\text{with } d_{\text{Chamfer}}(\mathfrak{X}^t, \mathfrak{X}^e) = \frac{1}{|\mathfrak{X}^t|} \sum_{x_i^t \in \mathfrak{X}^t} \min_{x_j^e \in \mathfrak{X}^e} \|x_i^t - x_j^e\|_2.$$

We select four seed points from $\mathfrak{X}^t$ of each fiber and identify the pathway that gives the minimum ϵ as $\mathfrak{X}^e$. Notice that the symmetrized Chamfer distance can be very large if the filter, initiated at one fiber of a configuration, does not capture the underlying diffusion profile around the fiber intersection and traces the other fiber. For completeness, we also find these "misidentified configurations" and report their percentage.

Table I shows the mean and standard deviation of ϵ for the aforementioned methods as well as the percentages of the misidentified configurations at different SNRs. Although the spatial tracking errors seem to be comparable as both methods achieve sub-voxel accuracy, our ODF-based method outperforms filtered two-tensor tractography at all levels of SNR by achieving a reduction in mean ϵ of 0.05 to 0.27 voxels. Similarly, the proposed method misidentifies a smaller number of configurations, i.e., at most 7% of the configurations, as opposed to 7%-20% when SNR $\neq 5$, and 10% versus 28% when SNR $= 5$. These results demonstrate that by removing the dependency of the UKF on a more restrictive diffusion model, it is possible to resolve higher degrees of complexity and track more fibers with increased accuracy.

Fig. 1(b) shows four fiber configurations along with the true centerlines $\mathfrak{X}^t$ (shown in red) and the estimated centerlines $\mathfrak{X}^e$ (shown in blue and black) when SNR $= 10$. Both methods yield accurate results for the first two configurations, whereas for the last two configurations our method outperforms filtered two-tensor tractography by resolving the fiber crossings.

B. Experiments on Real Data

We test the proposed method on a human brain dataset containing structural, functional, and diffusion MR images provided for the Pittsburgh Brain Connectivity Challenge (PBCC Spring 2009).[1] The diffusion weighted images were acquired with a 128×128 image matrix, a spatial resolution of 2 mm, 68 slices each with a thickness of 2 mm, and a diffusion sensitization at $b = 1{,}500$ s/mm^2 applied along a set of 256 gradient directions with 29 baseline images.

We consider a region of interest (ROI) containing structures such as the corpus callosum (CC), cingulum (CG), corona radiata (CR) and superior longitudinal fasciculus (SLF). The integrity of these tracts, shown in Fig. 2(a) on a white matter atlas [14], plays a critical role in several neurological disorders. We use the fractional anisotropy image (provided in the dataset) as a mask for selecting locations with high anisotropy as starting points for our method. Fig. 2(b) shows the resulting tracts, which are consistent with the neuroanatomy. More specifically, one can see the anterior and posterior portions, i.e., the genu and the splenium, of the CC as well as the body connecting the two hemispheres. In addition, the CG bundle and parts of the CR and SLF are correctly delineated. These tracts pass through several regions including the supplementary motor area (SMA) and the occipital lobe (OL), which are placed in Fig. 2(b) by registering the automated anatomical labeling (AAL) atlas [15] to the structural image.

IV. Conclusion and Future Work

In this work, we extended the UKF framework, which was shown to be successful for simultaneous diffusion model estimation and tractography, to HARDI data characterized by ODFs. We considered the spherical harmonic representation of the HARDI signal as the state, enforced nonnegativity of the ODFs, and performed tractography using the directions at which the ODFs attain their peaks. We further reduced model dependency by automatically identifying the number and locations of the modes of the ODFs. Experiments demonstrate the advantages of our approach over filtered two-tensor tractography in terms of accuracy in tracking under noise and identification of fiber crossings. We conjecture that the UKF framework may also improve tracking speed with an accuracy comparable to those of the classical methods decoupling estimation and tractography. Future work includes investigating other state space representations that will formalize the UKF into an intrinsic (manifold-constrained) formulation [16], as discussed in [10] for the space of diffusion tensors.

References

[1] D. Tuch, "Q-ball imaging," *Magnetic Resonance in Medicine*, vol. 52, no. 6, pp. 1358–1372, 2004.

[2] I. Aganj, C. Lenglet, G. Sapiro, E. Yacoub, K. Ugurbil, and N. Harel, "Reconstruction of the orientation distribution function in single- and multiple-shell q-ball imaging within constant solid angle," *Magnetic Resonance in Medicine*, vol. 64, no. 2, pp. 554–566, 2010.

[3] P. Basser, J. Mattiello, and D. LeBihan, "Estimation of the effective self-diffusion tensor from the NMR spin echo," *Journal of Magnetic Resonance B*, vol. 103, no. 3, pp. 247–254, 1994.

[1] pbc.lrdc.pitt.edu/?q=2009a-home

TABLE I

PERFORMANCE OF TRACTOGRAPHY METHODS: MEAN AND STANDARD DEVIATION OF THE SYMMETRIZED CHAMFER DISTANCE (ϵ) BETWEEN TRUE CENTERLINES $\mathfrak{X}^t$ AND ESTIMATED CENTERLINES $\mathfrak{X}^e$, AND THE PERCENTAGE OF MISIDENTIFIED CONFIGURATIONS

Diffusion Model	**SNR**				
	40	**30**	**20**	**10**	**5**
Two-Tensor	0.42±0.90 (7%)	0.44±0.49 (8%)	0.57±0.56 (17%)	0.73±0.76 (20%)	0.67±0.57 (28%)
ODF	0.37±0.27 (5%)	0.35±0.17 (3%)	0.39±0.25 (5%)	0.36±0.20 (7%)	0.54±0.33 (10%)

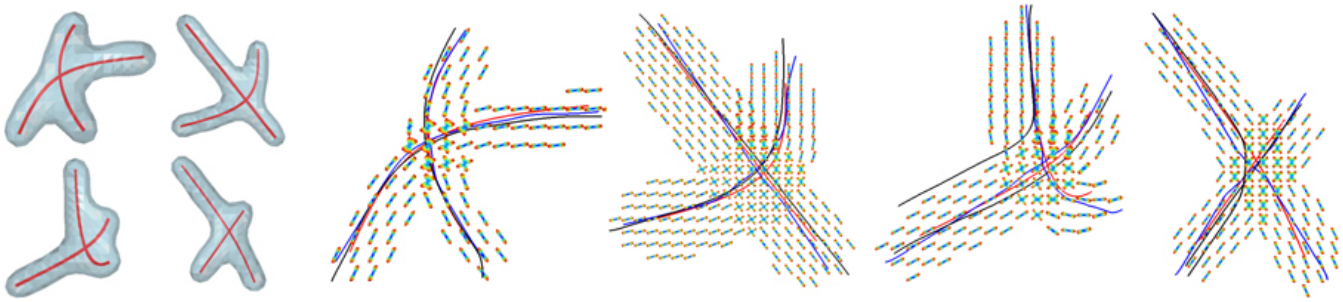

(a) (b)

Fig. 1. (a) Four synthetic fiber configurations with $\mathfrak{X}^t$ shown in red, (b) Tractography results at SNR $= 10$: $\mathfrak{X}^e$ shown in black (two-tensor) and in blue (ODF). Both methods produce accurate results for the first two configurations, whereas our method outperforms filtered two-tensor tractography for the last two configurations. [Note: The ODFs are color-coded (blue∼low, red∼high) and estimated offline for visualization from the HARDI data at SNR $= 40$.]

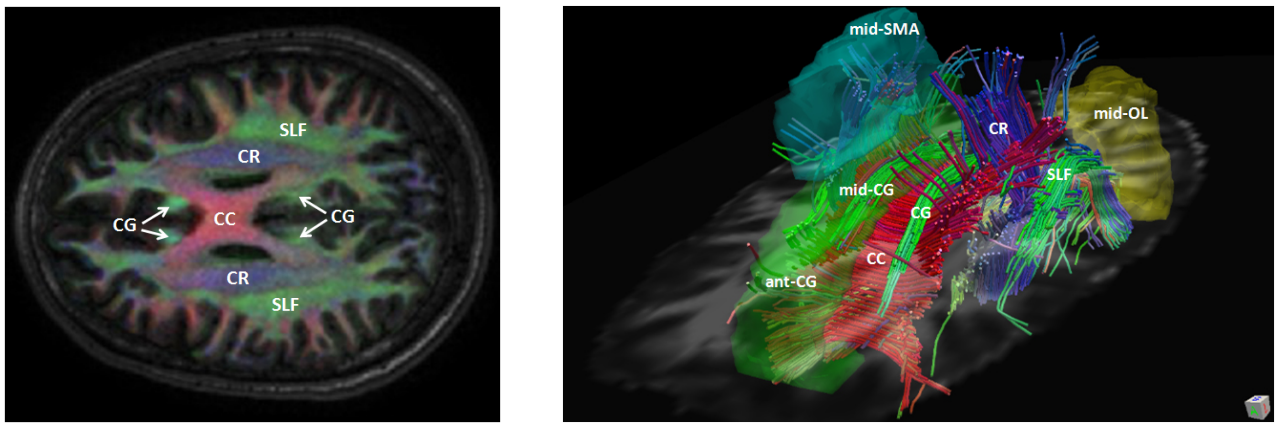

(a) (b)

Fig. 2. (a) An axial slice of the WM atlas (color-coded according to the principal diffusion directions) showing the corpus callosum (CC), cingulum (CG), corona radiata (CR) and superior longitudinal fasciculus (SLF), (b) Selected ROIs from the AAL atlas and tracts produced by filtered ODF tractography. These tracts (shown here cropped due the size of the initial ROI) pass through several cerebral regions including the SMA and OL.

[4] S. Mori and P. van Zijl, "Fiber tracking: principles and strategies - a technical review," *NMR in Biomedicine*, vol. 15, pp. 468–480, 2002.

[5] O. Friman, G. Farnebäck, and C.-F. Westin, "A Bayesian approach for stochastic white matter tractography," *IEEE Transactions on Medical Imaging*, vol. 25, no. 8, pp. 965–978, 2006.

[6] T. Behrens, H. J. Berg, S. Jbabdi, M. Rushworth, and M. Woolrich, "Probabilistic diffusion tractography with multiple fibre orientations: What can we gain?" *NeuroImage*, vol. 34, no. 1, pp. 144–155, 2007.

[7] M. Descoteaux, R. Deriche, T. Knoesche, and A. Anwander, "Deterministic and probabilistic tractography based on complex fiber orientation distributions," *IEEE Transactions on Medical Imaging*, vol. 28, no. 2, pp. 269–286, Feb. 2009.

[8] I. Aganj, C. Lenglet, N. Jahanshad, E. Yacoub, N. Harel, P. Thompson, and G. Sapiro, "A Hough transform global probabilistic approach to multiple-subject diffusion MRI tractography," *Medical Image Analysis*, vol. 15, no. 4, pp. 414–425, 2011.

[9] J. Malcolm, M. Shenton, and Y. Rathi, "Filtered multitensor tractography," *IEEE Transactions on Medical Imaging*, vol. 29, no. 9, pp. 1664–1675, 2010.

[10] G. Cheng, H. Salehian, M. Hwang, D. Howland, J. Forder, and B. Vemuri, "A novel unscented Kalman filter for tractography from HARDI," in *IEEE International Symposium on Biomedical Imaging*, 2012, pp. 534–537.

[11] H. Çetingül and R. Vidal, "Intrinsic mean shift for clustering on Stiefel and Grassmann manifolds," in *IEEE Conference on Computer Vision and Pattern Recognition*, 2009, pp. 1896–1902.

[12] M. Descoteaux, E. Angelino, S. Fitzgibbons, and R. Deriche, "Regularized, fast and robust analytical Q-ball imaging," *Magnetic Resonance in Medicine*, vol. 58, no. 3, pp. 497–510, 2007.

[13] A. Goh, C. Lenglet, P. Thompson, and R. Vidal, "Estimating orientation distribution functions with probability density constraints and spatial regularity," in *Medical Image Computing and Computer Assisted Intervention*, 2009, pp. 877–885.

[14] S. Mori, K. Oishi, and A. Faria, "White matter atlases based on diffusion tensor imaging," *Current Opinion in Neurology*, vol. 22, no. 4, pp. 362–369, 2009.

[15] N. Tzourio-Mazoyer, B. Landeau, D. Papathanassiou, F. Crivello, O. Etard, N. Delcroix, B. Mazoyer, and M. Joliot, "Automated anatomical labeling of activations in SPM using a macroscopic anatomical parcellation of the MNI MRI single-subject brain," *NeuroImage*, vol. 15, no. 1, pp. 273–289, 2002.

[16] B. Sipos, "Application of the manifold-constrained unscented Kalman filter," in *IEEE/ION Position, Location and Navigation Symposium*, 2008, pp. 30–43.